Chalcogenide Letters Vol. 19, No. 8, August 2022, p. 513 - 527

Synthesis and tribological properties of MXene/TiO_2/MoS_2 nanocomposite

X. Y. Gao, P. Lu, Z. M. Xu, G. G. Tang*
Changzhou Vocational Institute of Industry Technology, Changzhou, 213100, Jiangsu Province, China

In this work, novel MXene/TiO_2/MoS_2 heterojunction of flower-like MoS_2 decorated sheet-like MXenes were successfully fabricated by one-step hydrothermal approach using TiO_2 as the precursor, and systematically investigated by a series of characterizations (e.g. XRD, Raman, SEM, and TEM analysis). Furthermore, the tribological behaviour of MXene/TiO_2/MoS_2 heterojunction in liquid paraffin were extensively examined a ball-on-disk tribometer. The effects of applied load and rotational speed were also investigated. Compared with MXenes/MoS_2 nanocomposites, three-phase MXene/TiO_2/MoS_2 achieved better friction properties. Especially, when the mass ratio of MTM in base oil is 3wt%, the friction coefficient reaches the minimum value of 0.09. Additionally, the construction and excellent tribological properties of MXene/TiO_2/MoS_2 heterojunction would be beneficial for the design of novel nano-additives with 2D/2D structure for enhancing friction reduction and anti-wear, which also would expand their actual applications in the industry and agriculture.

(Received March 24, 2022; Accepted May 20, 2022)

Keywords: MoS_2, MXenes, Heterojunction, 2D/2D structure, Tribological properties

1. Introduction

As we know, Friction is universal in modern industry. Without friction, all mechanical components cannot work [1-3]. Furthermore, friction and wear are the major causes for the loss in materials and energies [4-6]. Generally, lubricants have been considered the most effective approach to reduce friction and wear, and prolong the service life of machines for energy loss [7-10]. Recently, many inorganic nanoparticles have been widely concerned as the promising and potential lubricant due to their excellent friction-reducing and anti-wear performances [11-14]. Therefore, exploring and developing novel inorganic nanoparticles or their composites for enhancing their tribological properties is the biggest challenge at present [15-18].

Nowadays, two-dimensional (2D) layered materials, like graphene and MoS_2, have gained considerable attention in the search for novel nano-lubricants to reducing friction and wear because their lamellar structures and easy interlayer sliding ascribed to the weak van der Waals interactions within their molecular layers [19-22]. In the characteristic layered structure of MoS_2, a Mo atomic layer sandwiched two S atomic layers. And the intralaminar of S–Mo–S layer is strong

* Corresponding author: xjing@ujs.edu.cn
https://doi.org/10.15251/CL.2022.198.513

covalent, while the interlayer of sandwiched structure is weak Van der Waals force, resulting the decrease in friction coefficient and possess enhanced reducing-friction and anti-wear properties [23-26]. More importantly, nano-sized MoS_2 show more excellent tribological properties compared to commercial MoS_2, which can be applied in harsh working environments. Recently, many previous researches indicated the modification of micro/nano-scale MoS_2 with introduction of other semiconductor nanoparticles can further improve its anti-friction and wear resistance [27-30]. Thus, MoS_2-incorporated composites composed of MoS_2 and other nanomaterials (e.g. graphene, WS_2, MoO_3 and h-BN, etc.) have been received extensive attention and synthesized through various methods, which also exhibited reinforcing and lubricating effects compared to that of pure MoS_2 [31-35].

Currently, MXenes, a novel 2D lamellar material, have attracted considerable attention and widely applied in lithium-ion batteries, super capacitors, heavy metal adsorption, and photocatalytic or electrocatalytic H_2 evolution because of graphene-like structure, hydrophilic surfaces, chemical stability, and outstanding electrical conductivities [36-38]. Furthermore, MXenes possess superior frictional properties and self-lubricating performance owing to its unique lamellar structure, high mechanical strength and low shear strength [39]. As expected, MXenes and its composites have been utilized as solid lubricant or lubricating additive for improving tribological properties. For example, the construction and macro-scale tribological properties of MXenes/MoS_2 using as a lubricating additive have been confirmed. On this basis, we tried to continue to composite TiO_2 nano materials to form three-phase MXene/TiO_2/MoS_2 nanocomposites, which has not been tried by predecessors.

Herein, the novel 2D/2D MXene/TiO_2/MoS_2 heterojunction were constructed and synthesized by one-step hydrothermal approach using MXenes as the precursor. And their frictional and wear behaviors were comparatively investigated by a ball-on-disk tribometer. Furthermore, the morphology and composition of the wear tracks were characterized by SEM, SMP and EDX technologies, which were conducted to understand their friction and wear mechanisms. Through the tribological property test and wear trace analysis, it can be determined that MXene/TiO_2/MoS_2 nano-composite has excellent lubrication performance as a solid lubrication additive. Thus, the construction and excellent tribological properties of MXene/TiO_2/MoS_2 heterojunction would be beneficial for the design of novel nano-additives with 2D/2D structure for enhancing friction reduction and anti-wear, which also would expand their actual applications in the industry and agriculture.

2. Experimental section

2.1. Synthesis of MXenes nanosheets

The MXenes nanosheets were synthesized by etching Al from Ti_3AlC_2 in HF solution. In a typical synthesis, Ti_3AlC_2 (5g) powders was immersed in HF solution (50 mL, 40%) for continuous stirring for 24 h at room temperature. After that, the as-prepared MXenes powder were obtained after repeated washings with DI water and ethanol to neutral, then drying at 80 ˚C in a vacuum oven for 8 h.

2.2. Synthesis of MXenes/TiO_2 heterojunction

In a typical synthesis, 100mg MXene was added to 15mL HCl solution with a concentration of 1.0m, and the solution was stabilized by ultrasonic agitation. Then 0.165g sodium fluoroborate ($NaBF_4$) was added to the solution, and the agitation continued for 30min, followed by 10min of ultrasonic agitation. The solution was transferred to a 100mL Teflon lined stainless steel reaction kettle and placed in an air blast oven at 180 degrees Celsius for 12h. At the end of the reaction, the supernatant was washed with deionized water and anhydrous ethanol for three times, centrifuged, and dried overnight at 60℃. Samples were collected and labeled as MT. To synthesize pure phase TiO_2, the reaction temperature only needs to be set at 210℃.

2.3. Synthesis of MXene/TiO_2/MoS_2 Nanocomposite

For the synthesis of MXene/TiO_2/MoS_2 Nanocomposite, 180mg sodium molybdate ($NaMoO_4 \cdot 2H_2O$) was added into 40mL deionized water, stirred and dissolved, then 360mg thiourea (CH_4N_2S) was added and continued stirring. After the drug was completely evenly dispersed, added 120mg MXene/TiO_2 synthesized above and stirred for 30 min. The solution was transferred into a 100mL Teflon lined stainless steel reaction kettle and placed in a blast oven at 200 ℃ for 24h. After the reaction, it was cooled naturally, washed with deionized water and anhydrous ethanol for three times respectively, centrifuged to remove the supernatant, and vacuum dried at 50℃ for 12h. Samples were collected and labeled MTM. For the synthesis of pure MoS_2, only the uniformly dispersed solution is directly transferred to the reaction kettle for hydrothermal reaction, without adding two-phase MXene/TiO_2. The synthesis diagram is shown in Fig. 1.

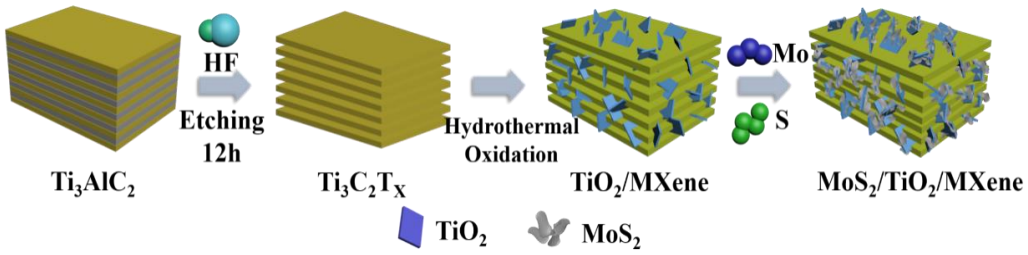

Fig. 1. Composite schematic diagram of MXene/TiO_2/MoS_2 nanocomposite.

2.3. Characterization

XRD (Bruker-AXS), XPS (Thermo Scientific K-Alpha+ system), Raman Microscope (DXR-Thermo Scientific), SEM (JEOL JXA-840A) and TEM analysis (JEOL JEM-2100) are performed to investigate the phase compositions, chemical states and microstructure of the as-prepared products.

2.4. Tribological Test

The friction reduction and anti-wear of pure base oil contained various nano-additives was investigated by a ball-on-disk tribometer (MS-T3001, China). In our experiments, liquid paraffin was selected as the lubricating oil. During experiments, the rotary velocity of the steel ball was kept 200 rpm, and the applied load was set to 2 N for 0.5h at room temperature. Also, different tribological variables including the additive concentration (0.7-7 wt %), rotary velocity (100-500

rpm), and applied load (2-6 N) were investigated. More importantly, all friction experiments were investigated three times, respectively. Afterwards, the surface roughness and elemental composition of the worn surfaces were quantified by non-contact optical 3D profilers (SMP, NT1100, Veeco WYKO, USA), Atomic Force Microscopy (AFM, MFP-3D, USA), and SEM-EDS analysis (HITACHI S-3400N, Japan).

3. Results and discussion

3.1. Nanostructure characterization of MXene/TiO_2/MoS_2

The phase composition of MXene/TiO_2/MoS_2 nanocomposites was determined by X-ray diffractometer (XRD). Fig.2 shows the XRD patterns of single-phase MoS_2, MXene, TiO_2, two-phase MXene/TiO_2 and three-phase MXene/TiO_2/MoS_2. As can be seen from Fig.2a, characteristic peaks of MXene(Ti_3C_2Tx) sample appear at 18.02°, 27.46°, 36.02°, 41.82° and 60.64°, corresponding to diffraction peaks of MXene at (004), (006), (101), (105) and (110) crystal planes respectively. Pure TiO_2 was obtained by hydrothermal oxidation of MXene at high temperature. As can be seen from the figure, diffraction peaks of samples at 25.38°, 37.8° and 48.08° correspond to crystal planes of (101), (004) and (200) of titanium dioxide. XRD patterns of MoS_2 samples show characteristic peaks at 17.26°, 32.46° and 57.9°, corresponding to diffraction peaks of (002), (100) and (110) crystal planes of MoS_2, respectively. In addition, the characteristic peaks of pure MXene and pure TiO_2 can be clearly observed from the XRD patterns of two-phase MXene/TiO_2, indicating that part of titanium dioxide was obtained by in-situ growth of MXene after hydrothermal oxidation. Then, the XRD patterns of three-phase MXene/TiO_2/MoS_2 were observed. The corresponding characteristic peaks of pure MXene, pure TiO_2 and pure MoS_2 could be obviously found on the XRD patterns of three-phase, indicating that the two-phase MXene/TiO_2 had a good composite with MoS_2, and the growth of crystal morphology was not affected in the composite process. Fig. 2b shows the XRD patterns of different percentages of MoS_2 in the composite phase MXene/TiO_2/MoS_2. It can be seen from the figure that with the increase of MoS_2 content, the characteristic peaks corresponding to the three pure phases of the sample do not change significantly. The XRD characterization of MXene/TiO_2/MoS_2 shows that the nanocomposite has been successfully synthesized.

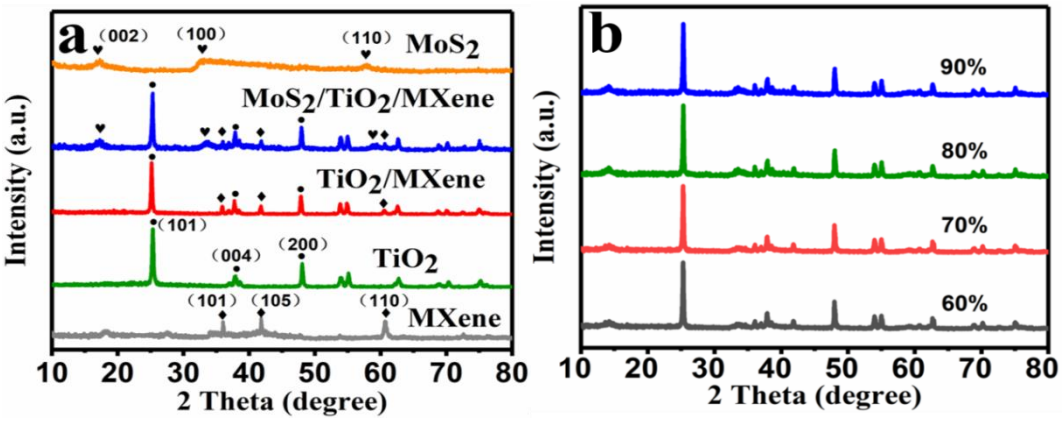

Fig. 2. XRD patterns of pure MXene, MoS_2, TiO_2, MXene/TiO_2 and MXene/TiO_2/MoS_2; (b) MXene/TiO_2/MoS_2 composites with different amount of MoS_2.

Raman spectroscopy was performed on pure and composite phase samples, as shown in Fig. 3. For pure MXene, characteristic peaks appear in 185cm^{-1}, 250cm^{-1}, 414cm^{-1} and 605cm^{-1}, which is due to the w1, w2, w3 and w4 vibration modes of Ti_3C_2. At the same time, an obvious characteristic peak appeared at 1600cm^{-1}, which was attributed to the plane vibration of sp2 hybrid C atom. For pure MoS_2, it can be seen from the figure that two obvious characteristic peaks are observed at 380.2cm^{-1} and 402.4cm^{-1}, respectively belonging to the in-plane E^1_{2g} and A_{1g} vibration modes of hexagonal MoS_2. The Raman spectrum of pure TiO_2 showed a characteristic peak at 142cm^{-1}, which was due to the in-plane $E_g(1)$ vibration mode of titanium dioxide and the characteristic peak at 394cm^{-1}, 515cm^{-1} and 635cm^{-1}, corresponding to the in-plane B_{1g}, B_{1g}/A_{1g} and $E_g(3)$ mode vibration of titanium dioxide . The characteristic peak of MXene/TiO_2 in two-phase MXene/TiO_2 retained the characteristic peak of titanium dioxide obviously, and the characteristic peak of MXene appeared at 190cm^{-1} and the characteristic peak of carbon layer appeared at 1600cm^{-1}. Finally, the Raman spectrum of the three-phase complex was observed, and it was obvious that the characteristic peak of molybdenum disulfide appeared at 378cm^{-1} while retaining the original Raman characteristic peak of the two-phase complex after loading molybdenum disulfide. The above analysis results are consistent with the structure of X-ray diffraction spectrum analysis, which basically indicates that we have successfully synthesized MXene/TiO_2/MoS_2 three-phase complex.

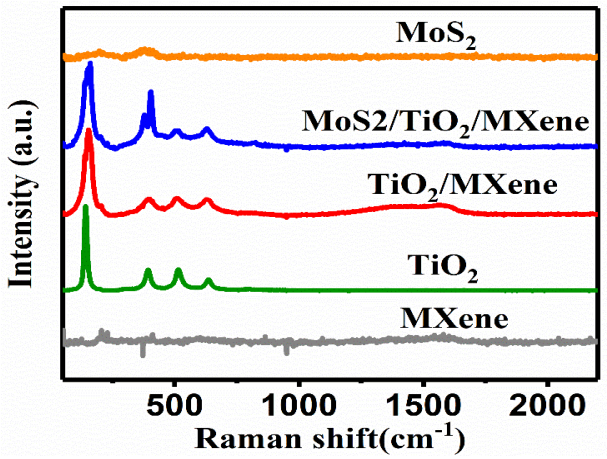

Fig. 3. RAMAN spectra of MXene, TiO_2, MoS_2, MXene/ TiO_2 and MXene/TiO_2/MoS_2 nanocomposite.

Figure 4 shows the morphology and microstructure of MXene/TiO_2, pure MoS_2 and three phase MXene/TiO_2/MoS_2. Fig. 4a is the SEM figure of MXene/TiO_2. It can be clearly seen from the figure that TiO_2 nanosheets grow in situ on the surface of MXene lamella after hydrothermal oxidation of MXene. Fig. 4b is a SEM image of the synthesis of single-phase molybdenum disulfide (MoS_2). Typical "flower-like" morphology of MoS_2 spheres can be clearly seen in the figure, which is made of MoS_2 nanosheets agglomerated together to form microspheres ranging in diameter from 1 to 5μm. Fig.4c and Fig.4d dare the microtopography of the three phase MXene/TiO_2/MoS_2. It can be seen intuitively that the MoS_2 nanosheet is supported on the TiO_2 nanosheet, and the exposed surface (101) of the TiO_2 nanosheet can be clearly observed. The

results showed that MoS_2 nanosheets were uniformly loaded on the (001) crystal plane of TiO_2 nanosheets. According to the results of scanning electron microscope, we successfully synthesized MXene/TiO_2/MoS_2 nanocomposite.

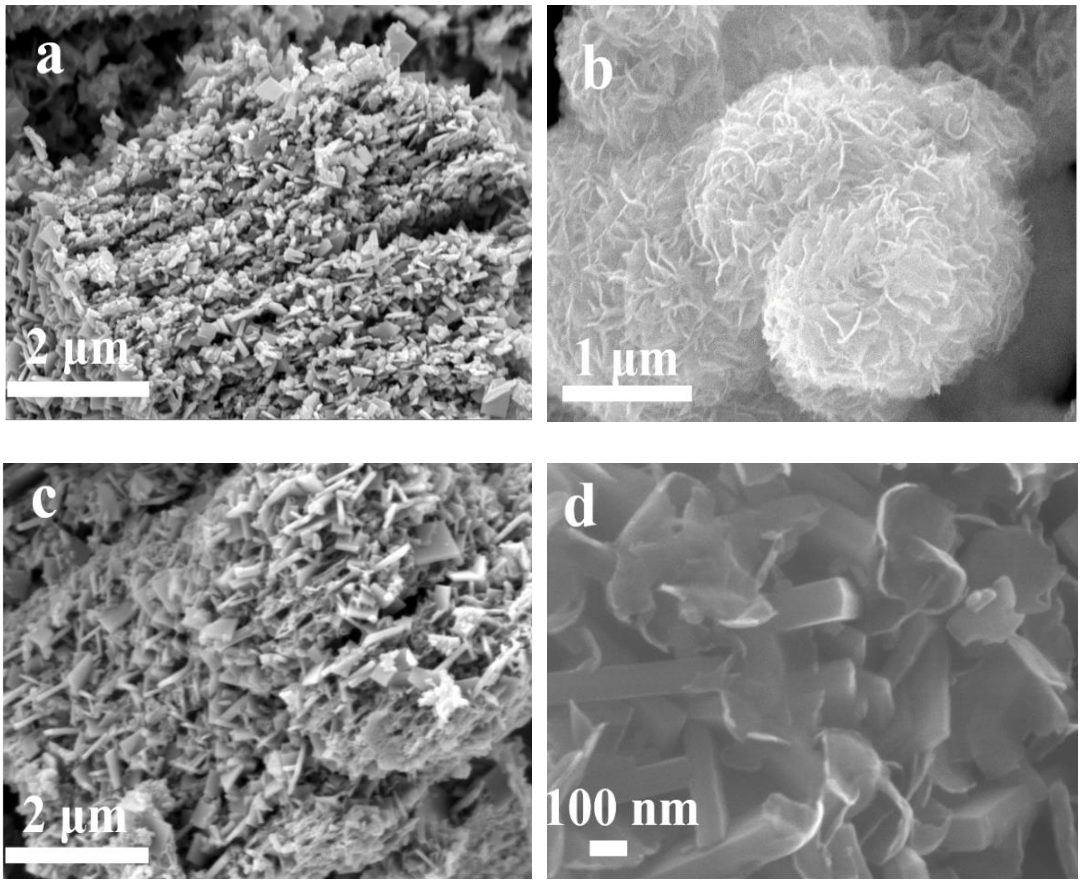

Fig. 4. SEM images of (a) MXene/TiO_2, (b)MoS_2, (c & d) MXene/TiO_2/MoS_2.

In order to observe the surface morphology and microstructure of the composite sample more intuitively, and to prove that a stable interface contact was formed between the molybdenum disulfide (MoS_2) nanosheet and TiO_2 laminate, transmission electron microscopy (TEM) was used to further characterize the composite sample (MXene/TiO_2/MoS_2), as shown in Fig. 5. As can be seen from Fig. 5a, MoS_2 nanosheets are attached to TiO_2 sheets, and the thickness of MoS_2 is uniform, and there is no agglomeration of MoS_2 nanosheets, which is the same as the result of SEM analysis. In addition, the high resolution transmission electron microscopy (HRTEM) Fig. 5b shows that the lattice fringe is 0.63nm, which corresponds to the (002) crystal plane of MoS_2, and the lattice fringe belonging to titanium dioxide is 0.35nm, which corresponds to the (101) crystal plane of titanium dioxide, found in the lattice fringe of MoS_2. This is consistent with the XRD analysis.

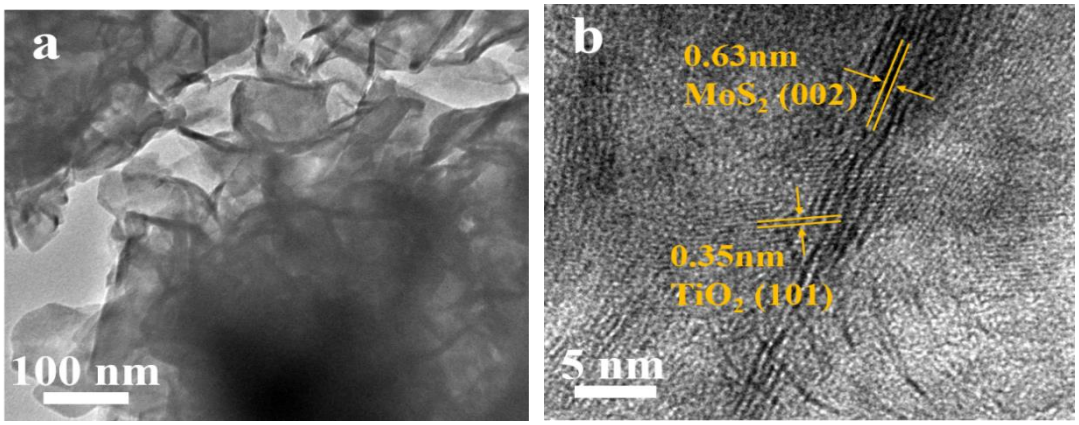

Fig. 5. TEM images of MXene/TiO_2/MoS_2.

In order to explore the tribological properties of three-phase MXene/TiO_2/MoS_2 nanocomposites, their friction coefficients were tested under the same experimental conditions. As shown in Fig. 6a, the corresponding friction coefficients of three-phase (MXene/TiO_2/MoS_2) composites in the tribological tests were far lower than those of pure oil, pure MoS_2 and two-phase (MXene/TiO_2) composites. It shows that the lubricating performance of MTM additive oil is obviously higher than that of pure oil, single phase MoS_2 and MT additive oil. Compared with MoS_2/MXene nanocomposites in the previous chapter, the friction coefficient of three-phase MXene/TiO_2/MoS_2 is significantly lower than that of MoS_2/MXene. Next, different contents of MXene/TiO_2/MoS_2 nanocomposites were added to the base oil in order to explore the optimal oil-material ratio of MXene/TiO_2/MoS_2 nanocomposites in the base oil, as shown in Fig. 6b. The friction properties of MTM nanocomposites were tested at different addition levels (0.7wt%, 1wt%, 3wt%, 5wt% and 7wt%). As can be seen from the friction coefficient in the figure, when the mass ratio of MXene/TiO_2/MoS_2 in the base oil is 3wt%, the corresponding friction coefficient is 0.09. In order to further analyze the tribological properties of MXene/TiO_2/MoS_2 composites, the effects of rotational speed and load on the tribological properties of solid lubrication additives were studied. First, we tested the friction coefficients of pure oil, single-phase MoS_2, composite phase MXene/TiO_2 and three-phase MXene/TiO_2/MoS_2 complex under different loads at the same speed of 300rpm and the optimal oil-material ratio of 3wt%. The results are shown in Fig. 6c. We observed that the corresponding friction properties of single-phase and composite phase were the best when the load was 5N. Note Lubricating oil is suitable for the friction environment with a load of 5N. In addition, under the same load, the friction coefficient of pure oil, single-phase MoS_2 and composite phase lubricating oil is still decreasing, indicating that under different friction environments, composite phase additive lubricating oil is still superior to single-phase additive lubricating oil. At the same time, we also controlled the same load and made the lubricating oil perform friction experiments at different rotational speeds. The measured results are shown in Fig. 6d. When the rotational speed increases from 100rpm to 500rpm, the friction coefficient of single-phase MoS_2 and composite phase (MTM-5) lubricating oil also changes regularly. And at the same speed, the friction coefficient of pure oil, single phase and compound phase lubricating oil still shows a decreasing law, which is the same as the result obtained under load. Combined

with the results of the above tribological properties test, we can come to the conclusion that the tribological properties of MXene/TiO_2/MoS_2 nanocomposites are obviously better than single-phase MoS_2 and composite MoS_2/MXene, indicating that the tribological properties of MoS_2/MXene are indeed greatly improved and improved after the composite TiO_2.

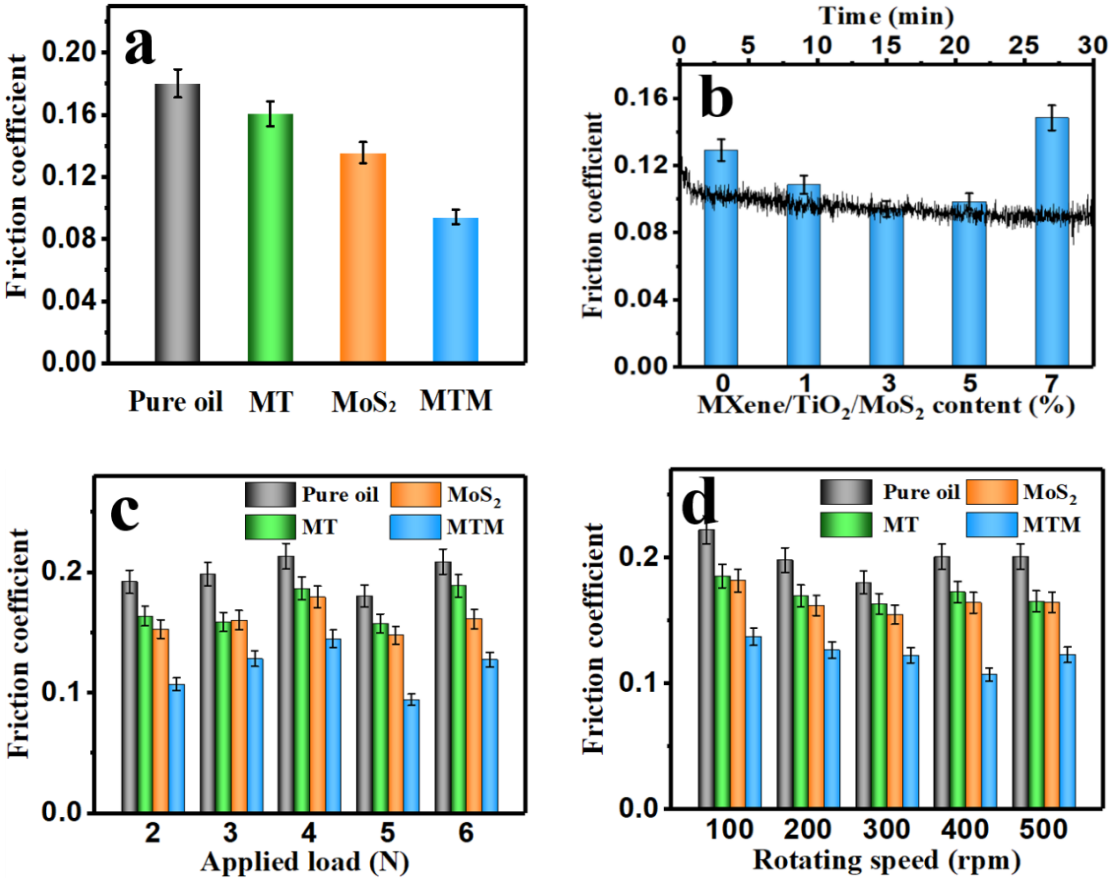

Fig. 6. (a) Friction coefficient of liquid paraffin contained with various oil additive; (b) Friction coefficient of liquid paraffin contained with different MXene/TiO_2/MoS_2 composites additive; Variations of mean friction coefficient of paraffin with different additive (c) increasing load (2-6 N), (d) under diverse speeds (100-500 rpm).

In order to further evaluate the wear reduction performance of MXene/TiO_2/MoS_2 nanocomposites as lubricating oil solid additives, we tested the circular steel plate with pure oil, single-phase MoS_2, composite phase MXene/TiO_2 and three-phase MXene/TiO_2/MoS_2 under the conditions of 5N load, 300rpm and 3wt% addition, and observed the wear marks on the surface of the circular steel plate by scanning electron microscopy which is shown in Fig. 7. Fig. 7a is the wear mark diagram of pure oil test. As we have introduced in the previous chapter, the wear mark on the surface of steel disk is more obvious, and there are obvious furrows and grooves on the surface, accompanied by some scratches, indicating that the lubrication performance of pure oil is poor without any solid lubrication additives. Fig. 7b shows the wear marks of composite phase MXene/TiO_2 additive lubricating oil after friction test. In the figure, it can be seen that the wear

marks on the surface of the steel plate are significantly improved, with no obvious deep furrows and relatively shallow wear marks, but there are a lot of obvious scratches. This result indicates that MXene/TiO_2 has a certain degree of wear reduction effect. However, the wear reduction effect is not obvious, which is consistent with the friction coefficient of friction test, because the friction coefficient of MXene/TiO_2 is only slightly decreased compared with pure oil. Fig. 7c shows the wear marks of pure MoS_2. From the wear marks alone, the wear reduction effect of Molybdenum disulfide is obvious. Fig. 7d is the wear pattern of three-phase MTM. Compared with the wear pattern of pure oil, pure MoS_2 and two-phase MT, the wear pattern of three-phase MTM is significantly smaller in width and depth, and the wear surface is very smooth with only slight dents and scratches. The results show that the three phase MTM solid additive has better antifriction performance in paraffin oil. The above results are also consistent with those of friction properties.

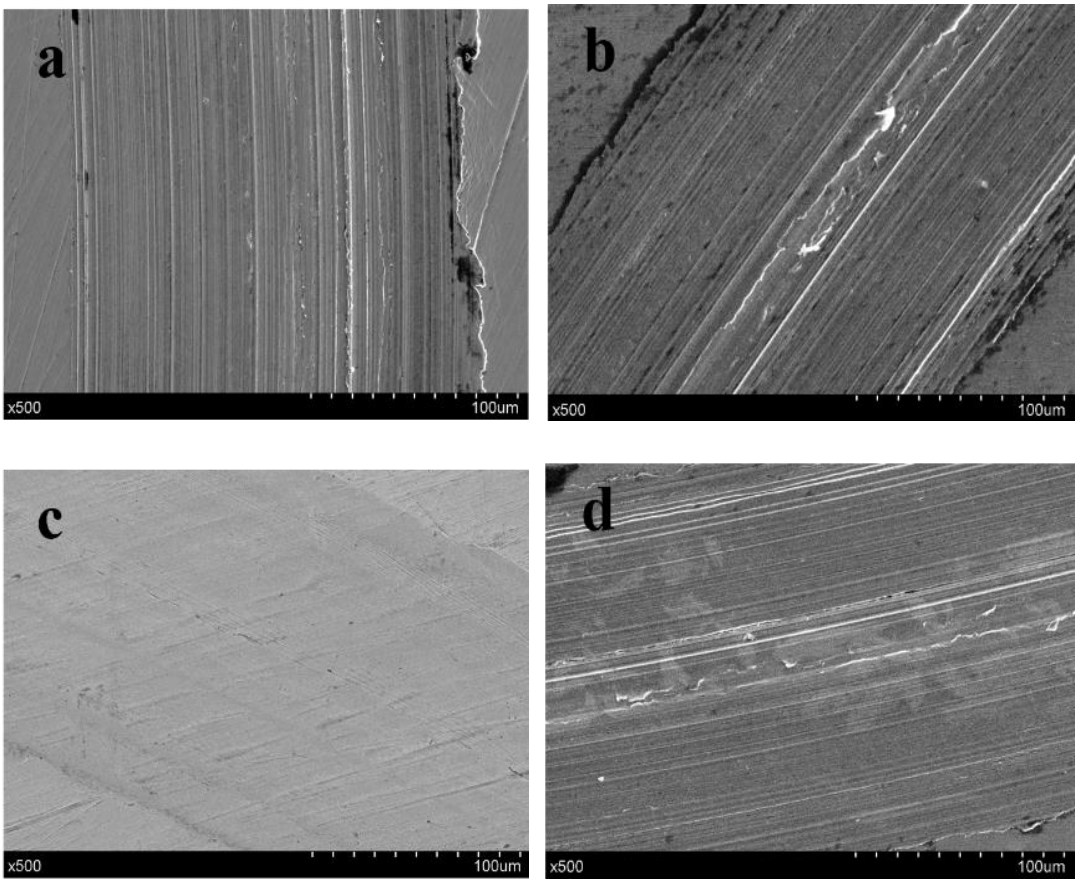

Fig. 7. SEM images of worn surfaces of (a) liquid paraffin, and liquid paraffin contained with (b) MXene/TiO_2; (c) MoS_2 and (d) MXene/TiO_2/MoS_2 composites.

We analyzed the depth and width of the wear marks of the above circular steel disk using a non-contact ultra-depth of field 3D microscope, as shown in Fig. 8. In the figure, we can see that the depth and width of pure oil wear marks are 7.549μm and 283.4μm. The wear depth and width of MXene/TiO_2 composite phase are 3.166μm and 228.8μm respectively. The depth and width of

wear marks corresponding to MoS_2 additive lubricating oil are 2.774μm and 229.7μm, respectively. By comparing the two before and after, we can see that the wear reduction effect of composite phase MT is not obvious. We then observed the depth and width of the wear trace corresponding to the three-phase MTM additive lubricating oil. The depth and width of the wear trace were significantly reduced, corresponding to 1.41μm and 207.3μm respectively, indicating that the wear reduction effect after the three-phase composite is very obvious, and it can also be determined that TiO_2 nanosheets play a crucial role in the friction test.

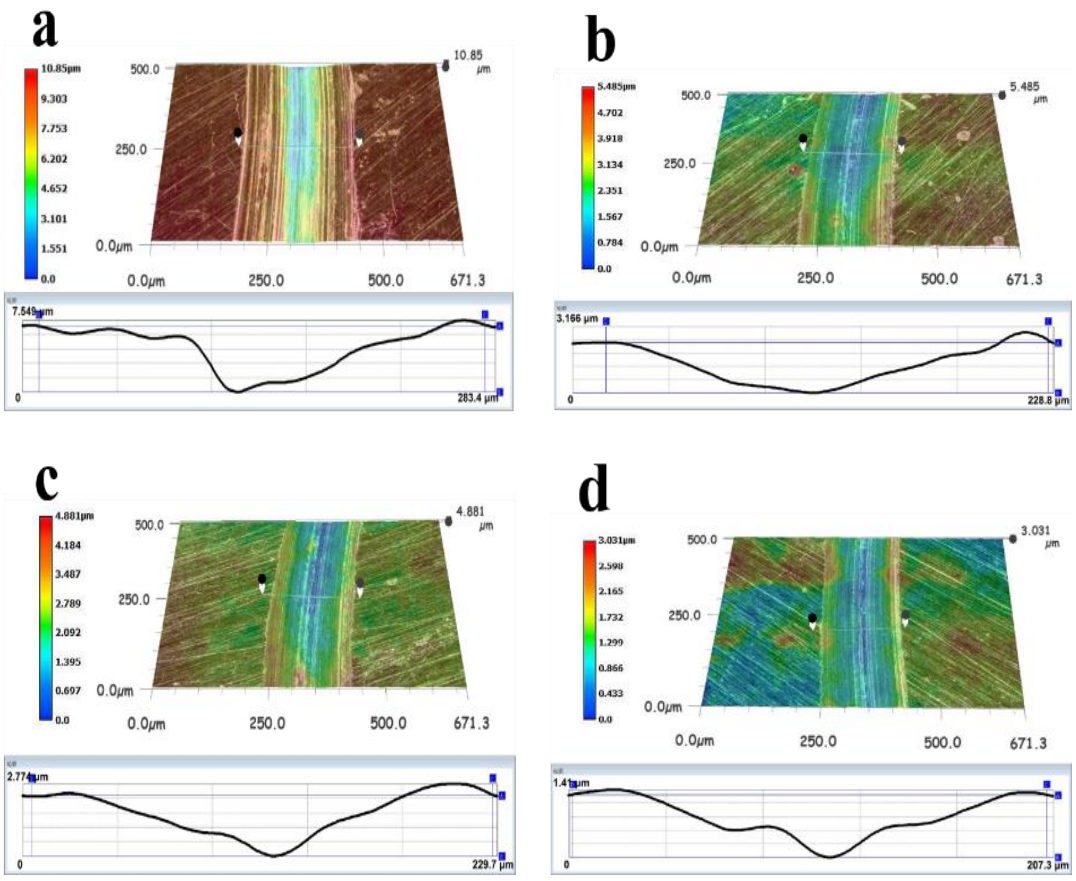

Fig. 8. Noncontact three-dimensional images of worn surfaces of (a) liquid paraffin; and liquid paraffin contained with (b) MXene/TiO_2; (c) MoS_2 and (d) MXene/TiO_2/MoS_2 composites.

In order to more intuitively observe the micro-morphology of indentations and furrows in the wear marks, we selected part of the surface of the wear marks as observation points for atomic force microscopy (AFM) analysis, and the results are shown in Fig.9. Fig. 9a shows the surface topography of the polished circular steel disk. It can be seen that the surface of the polished and polished steel disk is relatively smooth, with only nano-level fluctuations and bumps. Fig. 9b shows the microscopic morphology of the wear marks of pure oil lubricant. The dents in the wear marks are clearly visible and have a large depth. Fig. 9c shows the morphologies of wear marks of composite phase MXene/TiO_2/MoS_2 additive lubricating oil. Most of the wear marks are furrow shaped without large indentations, and the depth of the furrow is only about 1.1μm, far less than

the indentation depth of pure oil lubricant. The above results are in good agreement with the 3D profile of the wear marks and the results of friction performance analysis.

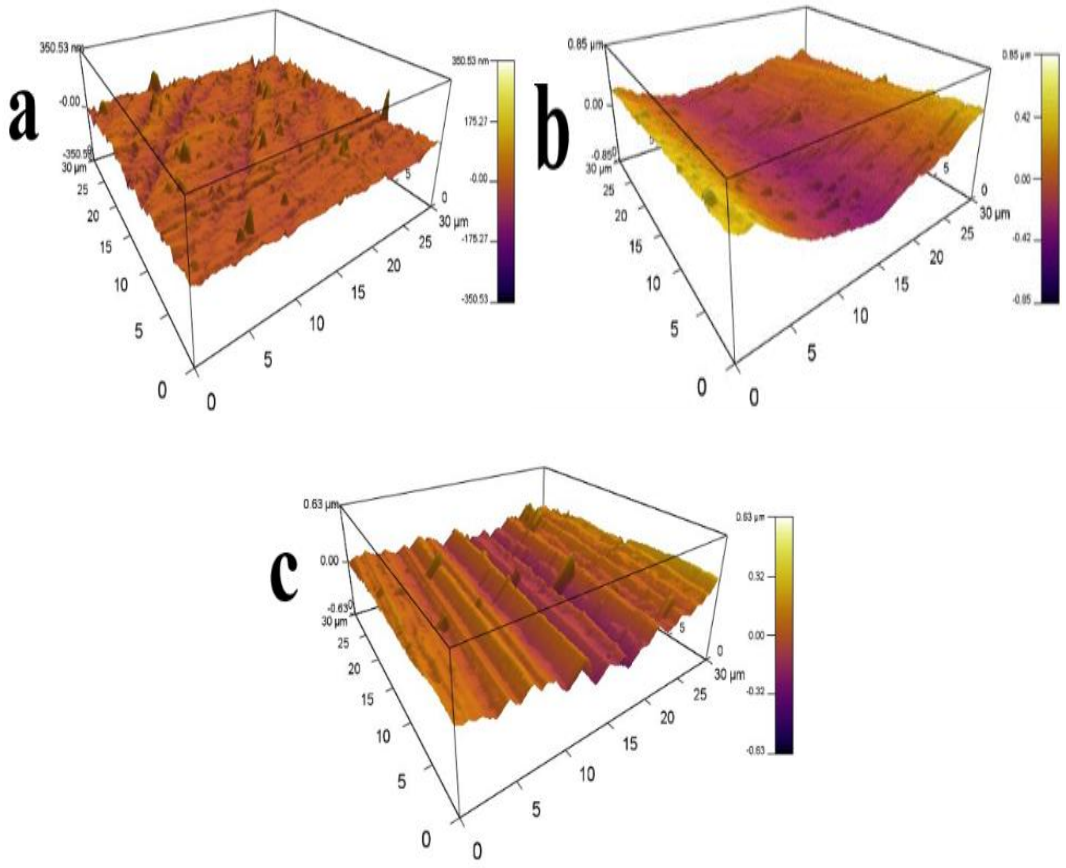

Fig. 9. AFM patterns of (a) steel disc surface, worn surfaces of (b) MoS_2 and (c) MXene/TiO_2/MoS_2 composites.

Through the tribological property test and wear trace analysis, it can be determined that MXene/TiO_2/MoS_2 nano-composite has excellent lubrication performance as a solid lubrication additive. Therefore, in order to further understand the lubrication mechanism of MoS_2/MXene in the lubrication process, ultrasonic cleaning was carried out on the wear surface of the steel disk tested for lubrication, and then EDS analysis was carried out on the wear surface to detect the element residues on the wear surface. As shown in Fig. 10, Fig. 10a and b are the wear marks of pure oil and MXene/TiO_2/MoS_2 steel disk respectively, and Fig. 10c and d are corresponding EDS energy spectrum respectively. With pure oil lubricant friction test after grinding crack (Fig. 7a) than can be found that adding a three-phase MTM lubricant, the surface of the grinding crack contains a certain amount of C, Mo, S, O and Ti element, shows that in the process of friction test, three-phase MTM nano lamella in external loads and under the action of shear force, also be a lubrication coating on the contact surface, To prevent further contact on the surface of steel and steel plate, in addition, MoS_2 and TiO_2 nanometer piece in the process can produce synergies, rules of nanometer titanium dioxide square piece in friction process has played a very good role of

"sliding", shows that three-phase complex multiple layer structure in enhancing the effect of sliding friction, have the effect of antifriction and antiwear, The friction mechanism is shown in Fig. 10e.

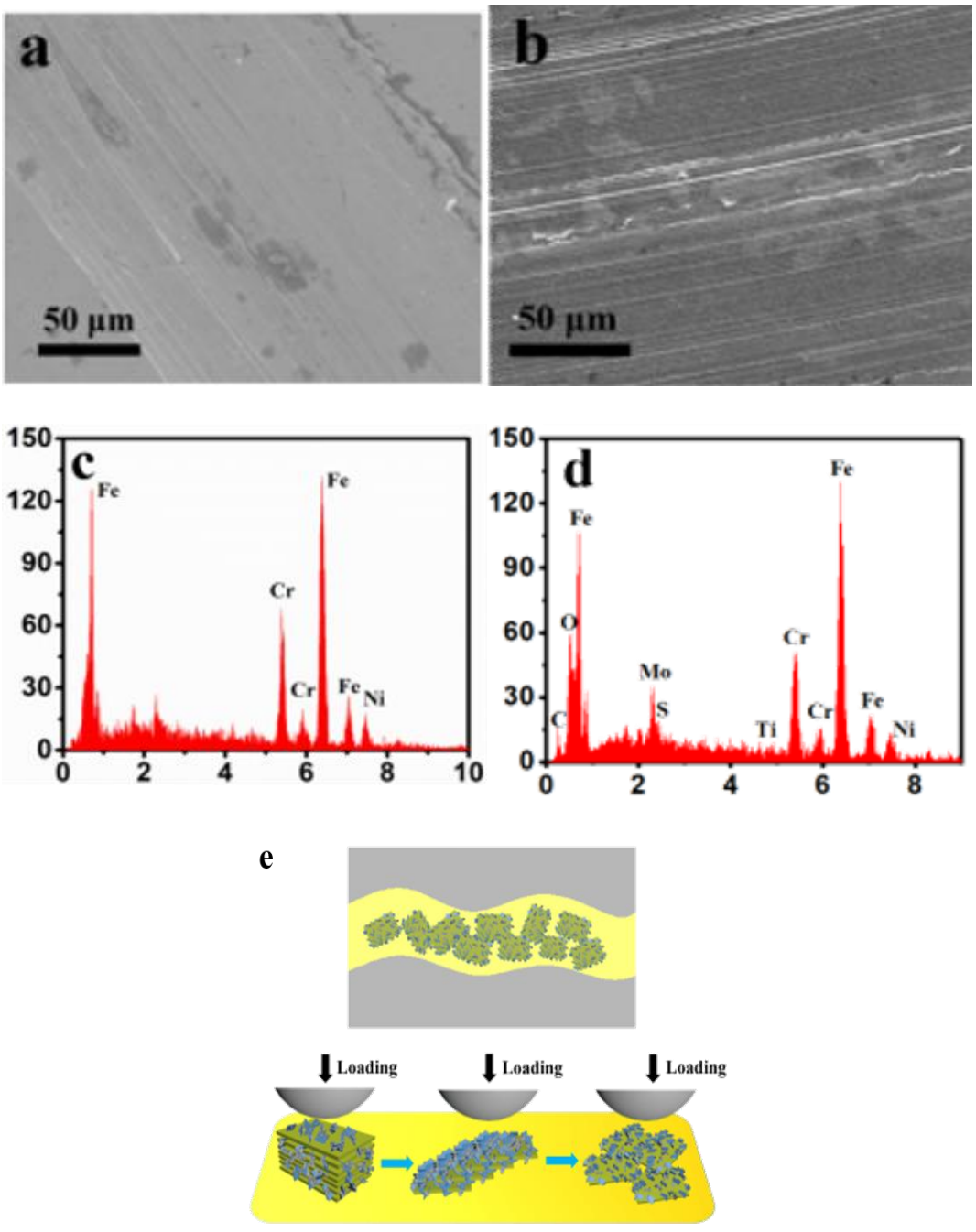

Fig. 10. SEM images and EDS of worn surfaces of (a, c) liquid paraffin and (b, d) MXene/TiO_2/MoS_2 composites, the tribological mechanism of MXene/TiO_2/MoS_2 additive in liquid paraffin (e).

4. Conclusions

Novel MXene/TiO_2/MoS_2 heterojunction of flower-like MoS_2 decorated sheet-like MXenes were successfully constructed and synthesized by one-step hydrothermal approach in the presence of MXenes, which was applied directly as a novel lubrication additive for tribological studies of liquid paraffin. The characterization results indicate that MoS_2 nanosheets were uniformly loaded on the (001) crystal plane of TiO_2 nanosheets and flower-like MoS_2 nanosheets evenly scattered on the surface of MXene layers. Furthermore, the tribological behavior of MXene/TiO_2/MoS_2 heterojunction in liquid paraffin were extensively examined a ball-on-disk tribometer, which indicate the friction and wear was significant decreased with introduction of MXene/TiO_2/MoS_2 heterojunction.

Compared with MoS_2/MXene nanocomposites, three-phase MXene/TiO_2/MoS_2 achieves lower friction coefficient. Especially, when the mass ratio of MTM in base oil is 3wt%, the friction coefficient reaches the minimum of 0.09. These results distinctly demonstrated MXene/TiO_2/MoS_2 heterojunction as lubricant additives in liquid paraffin exhibited superior antifriction and wear resistant, would be beneficial for the design of novel nano-additives with 2D/2D structure for enhancing tribological properties.

Acknowledgements

Our research project was sponsored by National Natural Science Foundation of China (51672113, 21975110 and 21972058), and Primary Research & Development Plan(social development project) of Zhenjiang (SH2019016).

References

[1] Y.F. Zuo, J. Mei, X.A. Zhang, C.H.T. Lee, IEEE Trans. Power Electron. 36 (2021) 716-726; https://doi.org/10.1109/TPEL.2020.3000656

[2] W.T. Zhu, L.C. Guo, L.B. Shi, Z.B. Cai, Q.L. Li, Q.Y. Liu, W.J. Wang, Wear 398 (2018) 79-89; https://doi.org/10.1016/j.wear.2017.11.023

[3] G.Y. Pan, X.M. Zhang, P. Liu, L. Chen, J. Vib. Control. (2020) 1077546320959517.

[4] M.J. Zhang, B.B. Chen, Z. Dong, S. Wang, X. Li, Y.H. Jia, F.Y. Yan, Polym. Compos. 41 (2020) 3768-3777; https://doi.org/10.1002/pc.25674

[5] R. Rattan, J. Bijwe, Tribol. Lett. 67 (2019) 36; https://doi.org/10.1007/s11249-019-1142-2

[6] H. Shi, S. Du, C. Sun, C. Song, Z. Yang, Y. Zhang, Materials 12 (2019) 45; https://doi.org/10.3390/ma12010045

[7] H. Mishina, J. JPN. Soc. Tribol. 57 (2012) 303-308.

[8] M. Umashankar, K. Annamalai, Mater. Today. 4 (2017) 9141-9146; https://doi.org/10.1016/j.matpr.2017.07.270

[9] R. Xia, X. Wang, B. Li, X. Wei, Z. Yang, Math Probl. Eng. 2019 (2019) 4191570; https://doi.org/10.1155/2019/4191570

[10] J. Teng, H. Li, G. Chen, J. Cent. South Univ. 22 (2015) 2875-2882; https://doi.org/10.1007/s11771-015-2820-3

[11] C.Y. Min, Z.B. He, H.J. Song, D.D. Liu, W. Jia, J.M. Qian, Y.H. Jin, L. Guo, Appl Sci-Basel. 9 (2019) 170; https://doi.org/10.3390/app9010170

[12] H.J. Song, Z.Q. Wang, J. Yang, Appl. Phy. A-Mater. 122 (2016) 933; https://doi.org/10.1007/s00339-016-0469-x

[13] Y.Y. Wu, W.C. Tsui, T.C. Liu, Wear 262 (2007) 819-825; https://doi.org/10.1016/j.wear.2006.08.021

[14] J. Khedkar, I. Negulescu, E.I. Meletis, Wear 252 (2002) 361-369; https://doi.org/10.1016/S0043-1648(01)00859-6

[15] A.D. Moghadam, E. Omrani, P.L. Menezes, P.K. Rohatgi, M Composites Part B. 77 (2015) 402-420; https://doi.org/10.1016/j.compositesb.2015.03.014

[16] Z.Y. Zhang, Y.T. Zhao, C.L. Wang, R. Tao, Z. fang, Y. Sun, X.Z. Kai, Mat Sci Eng A-Struct. 788 (2020) 139590; https://doi.org/10.1016/j.msea.2020.139590

[17] M.J. Zhang, B.B. Chen, Z. Dong, S. Wang, X. Li, Y.H. Jia, F.Y. Yan, Polym. Compos. 41 (2020) 3768-3777; https://doi.org/10.1002/pc.25674

[18] W.W. Song, X.J. Xu, S.R. Liu, J.F. Pu, H.F. Wang, Adv. Compos Lett. 29 (2020) 2633366X20927025; https://doi.org/10.1177/2633366X20927025

[19] X.H. Jia, J. Huang, Y. Li, J. Yang, H.J. Song, Appl. Surf. Sci. 494 (2019) 430-439; https://doi.org/10.1016/j.apsusc.2019.07.194

[20] Y.M. Zeng, F. He, L.N. Si, Y.J. Wang, Q. Wang, Mater. Res. Express. 6 (2019) 1150b4; https://doi.org/10.1088/2053-1591/ab4c73

[21] B.B. Chen, Y.H. Jia, M.J. Zhang, H.Y. Liang, X. Li, J. Yang, F.Y. Yan, C.S. Li, Composites, Part A. 122 (2019) 85-95; https://doi.org/10.1016/j.compositesa.2019.04.009

[22] B.B. Chen, X. Li, Y.H. Jia, L. Xu, H.Y. Liang, X.F. Li, J. Yang, C.S. Li, F.Y. Yan, Compos. Part A Appl. Sci. Manuf. 115 (2018) 157-165; https://doi.org/10.1016/j.compositesa.2018.09.021

[23] J. Xu, H. Tang, Y. Chu, C. Li, Rsc Adv. 5 (2015) 48492-48499; https://doi.org/10.1039/C5RA06999H

[24] X. Li, Z. Cao, Z. Zhang, H. Dang, Appl. Surf. Sci. 252 (2006) 7856-7861; https://doi.org/10.1016/j.apsusc.2005.09.068

[25] L. Rapoport, V. Leshchinsky, I. Lapsker, Y. Volovik, O. Nepomnyashchy, M. Lvovsky, R. Popovitz-Biro, Y. Feldman, R. Tenne, Wear 255 (2003) 785-793; https://doi.org/10.1016/S0043-1648(03)00044-9

[26] J. Xu, H. Tang, G. Tang, C. Li, Facile synthesis and characterization of flower-like MoS2 microspheres, Chalcogenide Lett. 11 (2014) 265-270.

[27] X.J. Hua, J.G. Sun, P.Y. Zhang, K. Liu, R. Wang, J.H. Ji, Y.H. Fu, J Tribol-T Asme. 138 (2016) 031302; https://doi.org/10.1115/1.4032522

[28] Y. Jiang, K. Shi, H. Tang, Y. Wang, Surf. Coat. Tech. 375 (2019) 334-340; https://doi.org/10.1016/j.surfcoat.2019.07.051

[29] G. Li, C. Li, H. Tang, K. Cao, J. Chen, F. Wang, Y. Jin, J. Alloys Compd. 501 (2010) 275-281; https://doi.org/10.1016/j.jallcom.2010.04.088

[30] G. Tang, F. Zhang, J. Xu, Micro Nano Lett. 14 (2019) 416-419;

https://doi.org/10.1049/mnl.2018.5420

[31] M.S. Zhang, B.B. Chen, J. Yang, H.M. Zhang, Q. Zhang, H. Tang, C.S. Li, RSC Adv. 5 (2015) 89682-89688; https://doi.org/10.1039/C5RA10308H

[32] R. Zhou, Z.P. Tong, G.F. Sun, Z.H. Ni, W. Zhang, Microstructure and wear behaviour of 38CrMoAl steel laser-processed with the addition of MoS2 or WS2, Lasers Eng. 41 (2018) 1-25.

[33] J. Xu, H. Tang, Q. Shi, C. Li, Synthesis and tribological properties of W-doped MoS2 nanoplates, Chalcogenide Lett. 12 (2015) 1-10.

[34] B.B. Chen, M.J. Zhang, X. Li, Z. Dong, Y.H. Jia, C.S. Li, Prog. Org. Coat. 147 (2020) 105767; https://doi.org/10.1016/j.porgcoat.2020.105767

[35] W. Song, P. Chen, J.C. Yan, W.S. Zhu, H.B. Ji, ACS Appl. Mater. Interfaces. 12 (2020) 29737-29746; https://doi.org/10.1021/acsami.0c03467

[36] C. Prasad, X.F. Yang, Q.Q. Liu, H. Tang, A. Rammohan, S. Zulfiqar, G.V. Zyryanov, S. Shah, J. Ind. Eng. Chem. 85 (2020) 1-33; https://doi.org/10.1016/j.jiec.2019.12.003

[37] D.Q. Li, X.F. Chen, P. Xiang, H.Y. Du, B.B. Xiao, Appl. Surf. Sci. 501 (2020) 144221; https://doi.org/10.1016/j.apsusc.2019.144221

[38] D.W. Rao, L.Y. Zhang, Y.H. Wang, Z.S. Meng, X.Y. Qian, J.H. Liu, X.Q. Shen, G.J. Qiao, R.F. Lu, J. Phys. Chem. C. 121 (2017) 11047-11054; https://doi.org/10.1021/acs.jpcc.7b00492

[39] X.H. Zhang, M.Q. Xue, X.H. Yang, Z.P. Wang, G.S. Luo, Z.D. Huang, X.L. Sui, C.S. Li, RSC Adv. 5 (2015) 2762-2767; https://doi.org/10.1039/C4RA13800G

[40] A. Mukherji, L. Saikia, R. Srivastava, Chem. Eng. J. 373 (2019) 1233-1246; https://doi.org/10.1016/j.cej.2019.05.133

[41] S. Bolar, S. Shit, J.S. Kumar, N.C. Murmu, R.S. Ganesh, H. Inokawa, T. Kuila, Appl. Catal. B-Env. 254 (2019) 432-442; https://doi.org/10.1016/j.apcatb.2019.04.028

[42] Y. Liao, J. Qian, G. Xie, Q. Han, W.Q. Dang, Y.S. Wang, L.L. Lv, S. Zhao, L. Luo, W. Zhang, H.Y. Jiang, J.W. Tang, Appl Catal B-Environ. 273 (2020) 119054; https://doi.org/10.1016/j.apcatb.2020.119054

[43] Y.L. Sun, Y. Sun, X. Meng, Y. Gao, Y. Dall'Agnese, G. Chen, C. Dall'Agnese, X.F. Wang, Catal. Sci. Technol. 9 (2019) 310-315; https://doi.org/10.1039/C8CY02240B

[44] W.Y. Yuan, L.F. Cheng, Y.R. An, S.L. Lv, H. Wu, X.L. Fan, Y.N. Zhang, X.H. Guo, J.W. Tang, Adv. Sci. 5 (2018) 1700870; https://doi.org/10.1002/advs.201700870